CHAPTER 6

EFFECTS OF AN OPEN-AIR ANNEALING ON THE PERFORMANCE OF THE BLEND OLED DEVICE

6.1 Annealing Process in OLED Technology

Annealing process is a promising method that can be used to enhance the performance of OLED device. Via annealing process, turn on voltage of OLED can be reduced [*Sepeai et al., 2009*], thus power consumption in the device operation can be saved. In particular, OLED devices that have annealed under an ambient hydrogen atmosphere exhibit smooth surface morphology. Smooth surface improves carrier diffusion at an organic-metal interface. Under certain annealing temperature, organic molecules rearrange themselves to a form much compact structure, which results in an efficient energy or charge transfer among molecules. Annealing process also has been used to reduce sheet resistance of a conducting polymer for an anode in an OLED fabrication [*Kim et al., 2003*]. Reduction in sheet resistance leads to an increase in the conductivity and luminance of the OLED device.

Usually an annealing process was performed in a controlled environment either in a vacuum [*Ribierre et al., 2010; Sun et al., 2005*] or an ambient inner gas [*Osipov et al., 2007*] to avoid an oxidation process. However, thermal treatment for an injection

layer is usually performed in air environment [*Choudhury et al., 2009; Li et al., 2007; Song et al., 2010*]. This annealing method is performed at low temperature and for a short period. Because of its simple processing method, an open-air annealing process has been performed on TPD:PBD:Alq_3 blend OLED. Effects on the open-air annealing to the performance of the device are discussed in this chapter.

6.2 Experimental

TPD:PBD:Alq_3 single layer OLEDs were prepared using the same method as described in the chapter 3. The devices were annealed at 100^{o}C in an open-air of 100K clean room environment. The annealing time was varied from 0, 10, 20 to 30 minutes. After the annealing process was performed, 100 nm top Al electrodes was deposited on the devices using a thermal evaporation technique. Meanwhile, thin films of the blend were deposited on cleaned glass slides and undergoing the same annealing process as the OLED devices.

The structural properties of the thin films were analyzed by FTIR (Perkin Elmer) and XRD (Siemens). Optical absorption and photoluminescence characteristics were obtained by UV-Vis-NIR (Jasco-V50) and luminescence spectrometer (Perkin Elmer LS 50B), respectively. The surface morphology and microscope images were obtained from atomic force microscope (AFM) and optical microscope of Tencor 6, respectively. The thickness of the thin film device was measured by a profilometer (Tencor 6). Current density-voltage-luminance (*J-V-L*) characteristics were measured using a chroma meter CS-200 (Konica Minolta) powered by a source measure unit (Keithley 2400). All characterizations of the device performance were carried out at room temperature without encapsulation.

6.3 Structural Study

FTIR transmittance peak of TPD:PBD:Alq_3 thin film with different annealing time is shown in Fig. 6.1 (a). As expected, all transmission peaks of each element in the blend were observed to remain without any significant shifting. It is observed that there is a slight reduction of transmittance peak at 1385 cm^{-1} and 1328 cm^{-1} after the blend film is annealed for 10 minutes. This reduction can be clearly been seen in a normalized FTIR spectra in Fig. 6.1 (b). At higher annealing time, the peak obtained increases until 30 minutes of annealing time. This indicates that, after 10 minutes of annealing, the absorption of molecular vibration increases which is due to more the formation of compact structure of molecule in the blend thin film. However, above this annealing time, the thin film exhibit reduction in the molecular absorption which can be related to degradation of the organic molecule. Similar pattern was observed at peaks of 1177, 1115, 1075, 1065, 1030 and 1007 cm^{-1} as shown in Fig. 6.1 (c). It is notice that there is no any additional oxygen molecule attached onto the organic blends even after the thin film was annealed above 10 minutes. This is because the oxygen molecule only cause an oxidative degradation at certain molecular groups which result in the reduction of FTIR absorption.

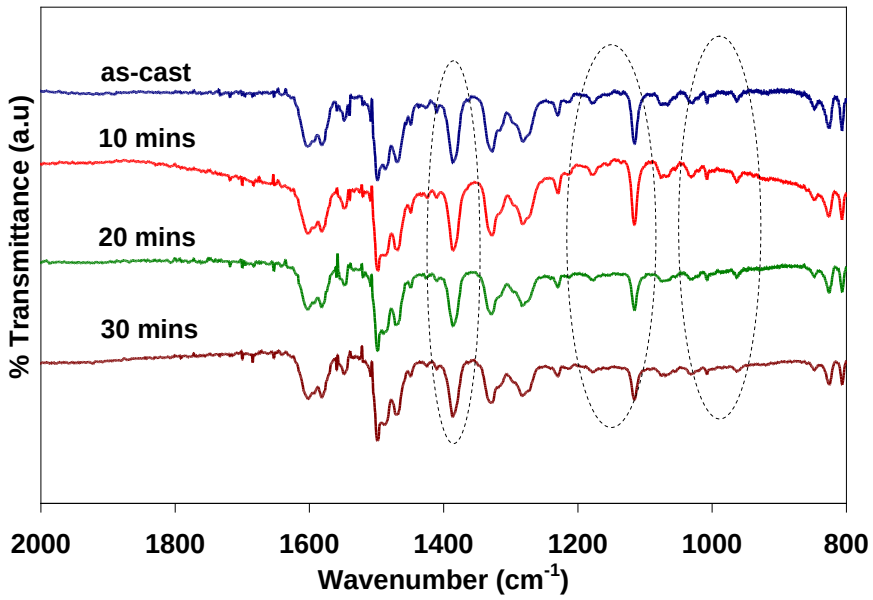
as-cast
10 mins
20 mins
30 mins
% Transmittance (a.u)
2000
1800
1600
1400
1200
1000
800
Wavenumber (cm-1)

(a)

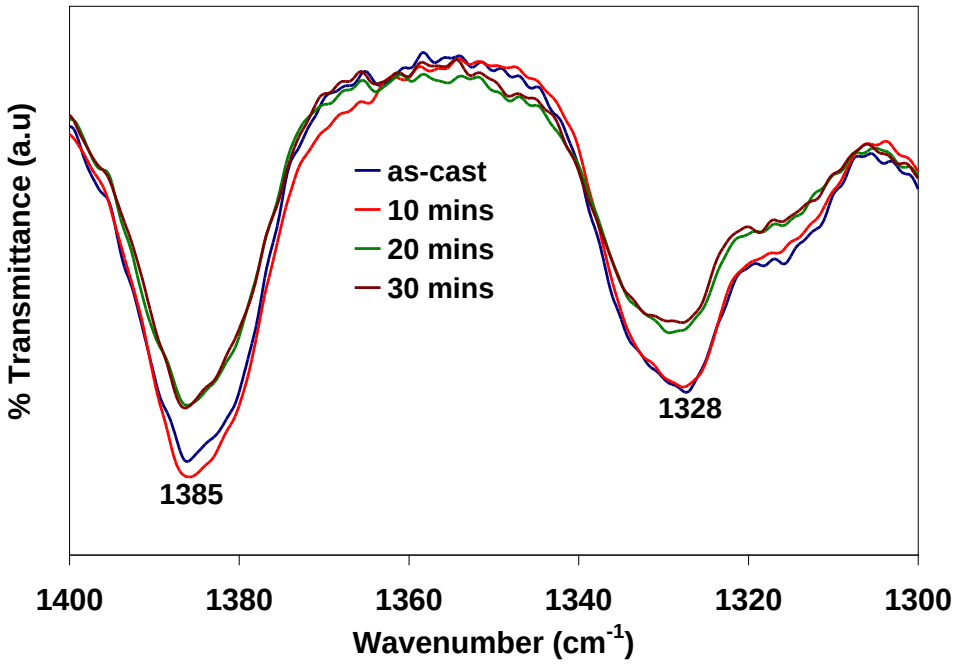
as-cast
10 mins
20 mins
30 mins
% Transmittance (a.u)
1385
1328
1400
1380
1360
1340
1320
1300
Wavenumber (cm-1)

(b)

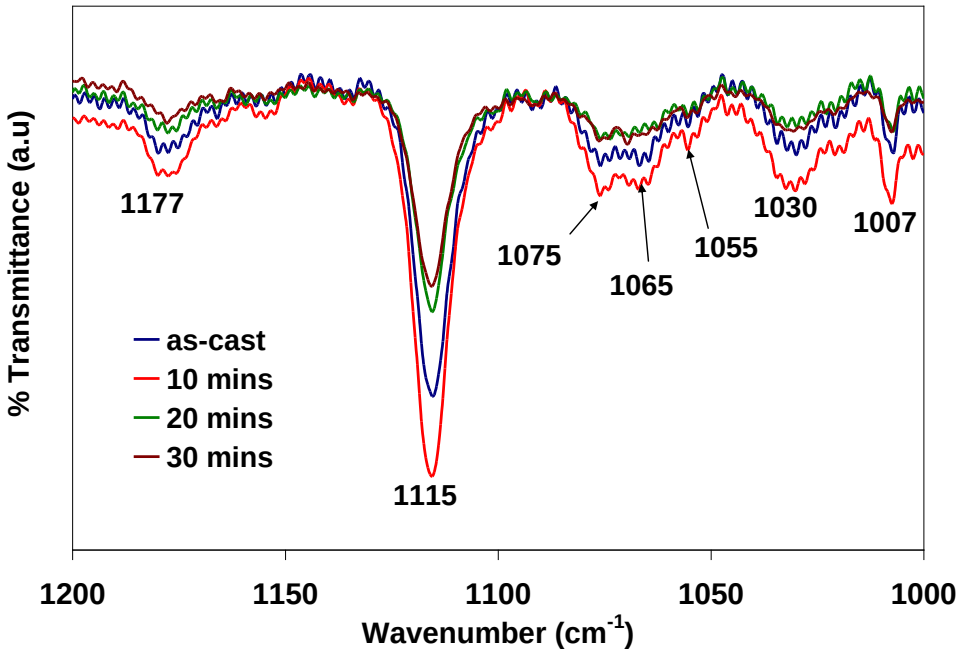

(c)

Figure 6.1: FTIR spectrum of TPD:PBD:Alq_3 thin film with different annealing process at range of (a) 2000 to 800 cm^{-1}, (b) 1400 to 1300 cm^{-1} and (c) 1200 to 1000 cm^{-1}

Fig. 6.2 shows the XRD pattern of the blend thin film annealed at different times. The existing of the broad peak centered at 25^o indicates that the blend film remains in the amorphous phase for all the thin films even that was annealed at higher annealing time. It can be expected that the annealing process can change the molecular arrangement of the organic thin film from amorphous into crystalline phase [*Park et al., 2010*]. However, one of the criteria that must be fulfilled in order for this transition to occur is that, the applied annealing temperature must exceed the glass transition temperature (T_g) of the material. From literature, the value of T_g for Alq_3, TPD and PBD is 175^{o}C [*Adachi et al., 1995*], 60^{o}C [*Tokito et al., 1997*] and ~60 ^{o}C [*Kulkarni et al., 2004*], respectively. Annealing at 100^{o}C may cause the structure of TPD and PBD molecules to change from amorphous to crystalline. However, the presence of Alq_3 molecule in such a blend leads to an increase in the T_g value of the blend films and makes them more thermally stable. Similar observation has been reported in [*Krieg et*

al., 1999] where the thermal stability of TPD has been improved by doping with high T_g material of fullerene C_{60}. It is noted that the thermal heating process performed in an open-air condition may cause oxidation. However the crystalline peak of oxide structure does not appear, indicating that the attached oxide is in an amorphous form. On the other words, the oxidation process is not very dominant and the oxygen molecule only cause degradation of the thin film annealed above 10 minutes as shown in the previous FTIR results.

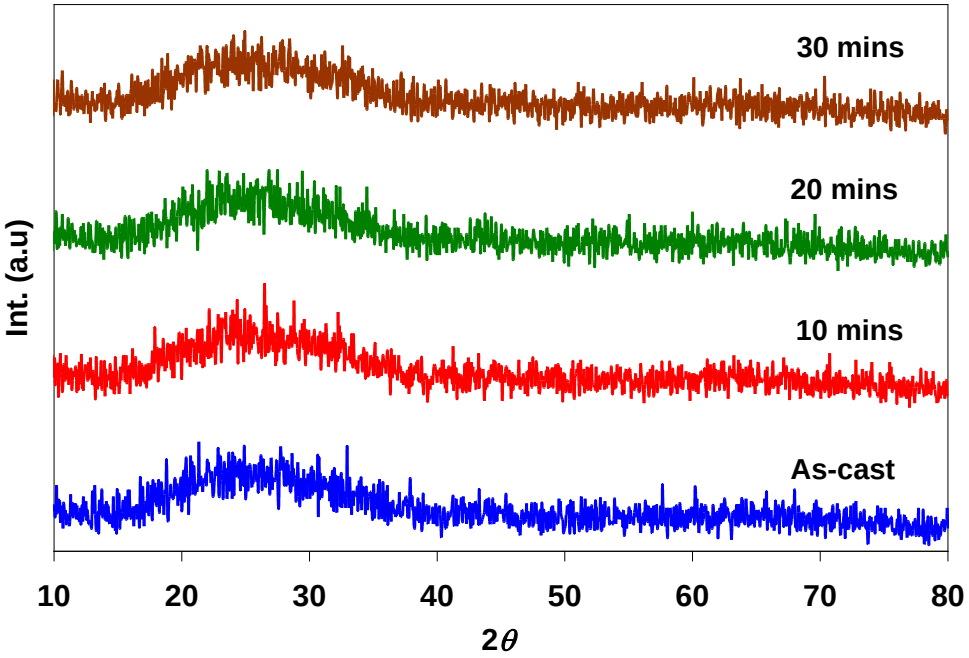

Figure 6.2: XRD pattern of TPD:PBD:Alq_3 thin film with different annealing time

6.4 Optical and Photoluminescence Study

Optical properties of the annealed blend thin film were characterized using UV-Vis spectrometer with the same setup as described in the previous Chapter 3. Fig. 6.3 shows the UV-Vis absorption of the blend thin film with different annealing times. The shape of the absorption spectra is observed to be similar for all thin films annealed at different annealing times. This indicates that the annealing process does not change the bonding at molecular level. There is one absorption peak in the visible region centered

at 310 nm and a shoulder at 370 nm which can be assigned to $\pi \rightarrow \pi^*$ electronic transition of the organic molecules. Absorption intensity for the as-cast and the 10 minutes annealed blend thin film observed to be almost similar. However, the spectra are observed to reduce for the thin film annealed at longer time. The absorption intensity of such thin films is also related to their thickness. The measured thickness of the blend thin films is shown in Table 6.1. At the annealing time of 10 minutes, the blend film exhibit almost the same thickness as that of the as-cast film. However, by increasing the annealing time, the molecules inside the blend thin film reorganize themselves to form a more compact structure, which lead to the decrease in thickness of the thin film. The decrease in the thickness, thus results in the reduction of the absorption intensity. The absorption spectrum at the shoulder region shows a small red-shift with the increase in the annealing time which may lead to a small decrease in the optical energy gap.

Table 6.1: Thickness measured of annealed blend thin film.

Annealing time (mins)	Thickness (nm)
0	83±1
10	79±1
20	65±3
30	56±4

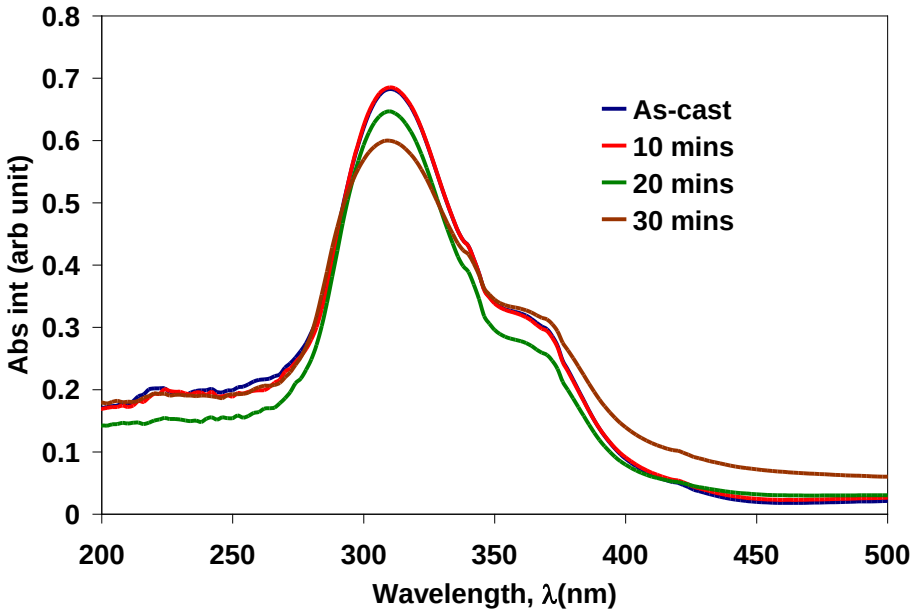

Figure 6.3: UV-Vis absorption of blend thin film with different annealing time

From the absorption spectra in Fig. 6.3, Tauc relation has been used to determine the optical energy gap, E_g of the annealed thin films. In Fig. 6.4, $(\alpha hv)^2$ against E plot of the blend thin film at different annealing time is shown. The extrapolation of the plot at $(\alpha hv)^2 = 0$ gives the optical energy gap. There is a small change in the value of energy gap for the blend thin film annealed at different annealing time. The value of the energy gap is 3.20±0.2 eV for the as-cast thin film, 3.19±0.2 eV for both the 10 and 20 minutes annealed thin films and 3.16±0.2 eV for the 30 minutes annealed thin film. The small decrease in the value of the energy gap is related to the improvement in the π→π interchain interaction which reduces the π→π* interaction [*Singh et al., 2005*]. This result also serves an evident that the molecules inside the blend thin film become denser when annealed at higher annealing time [*Muhammad & Sulaiman*]. However, one need to note that this reduction in the energy gap may not be so significant can be neglected as the reduction observed is too small (<0.5 eV).

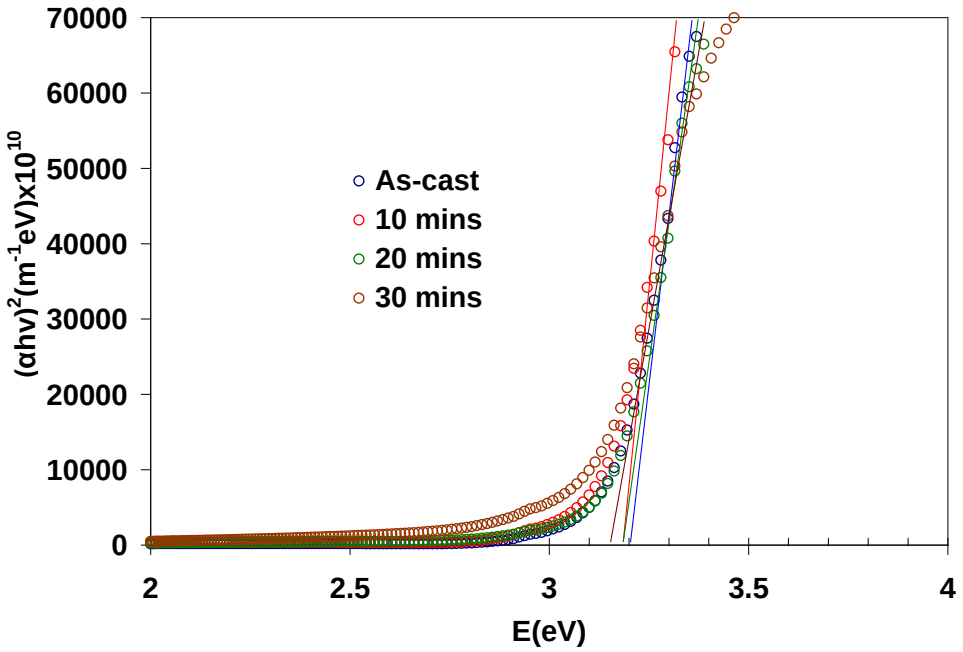

Figure 6.4: $(\alpha E)^2$ vs *E* plot of blend thin film at different annealing time

PL measurement was performed in room environment and the annealed thin films were excited under the excitation wavelength of 312 nm. Fig. 6.5 shows the PL of the blend thin film with different annealing time. The PL peak for the entire annealed thin films shows almost similar peak located around 516 nm. It can be suggested that a very small reduction in the energy gap obtained from the absorption results doesn't affect the PL peak position. The intensity of the PL spectra observed increases with longer annealing time. It is reported that the rearrangement of molecules leads to minimum potential energy among them in thin film, and it causes the PL intensity to increase [*Osipov, et al., 2007*]. Additionally, according to W.-I. Jeong et al, for thin film, the PL efficiency is largely influenced by the surface reaction, while for thicker films the optical effects such as wave guiding and interference, influence the PL efficiency to decrease to the apparent efficiency by about 20% [*Jeong et al., 2009*]. Besides, a more compact molecular structure reduces the non-radiative transition paths giving rise to the PL intensity. In short, the relation between absorption and PL intensity with annealing time is shown in Fig. 6.6

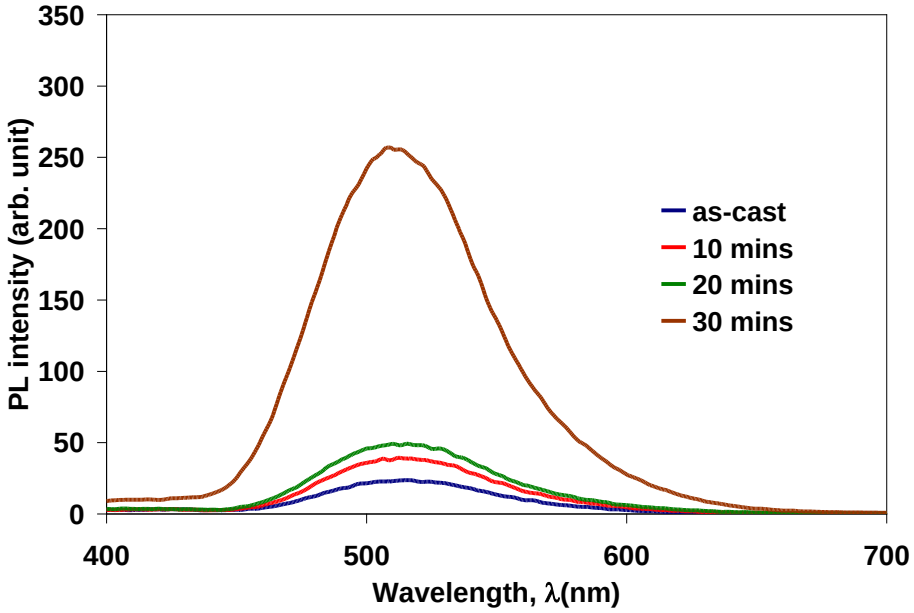

Figure 6.5: PL of blend thin film with different annealing time with excitation wavelength of 312 nm.

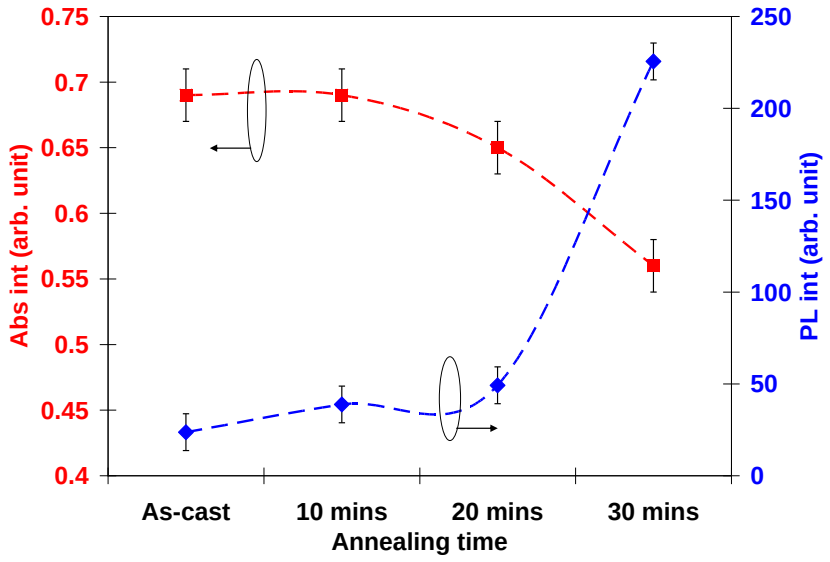

Figure 6.6: Absorption and PL intensity of annealed films with respect to annealing time

6.5 Surface Morphology Study

Surface profile of the thin film is one of the most important characterizations whenever an annealing process is performed. Atomic force microscopy (AFM) was carried out to investigate the surface morphology of the annealed thin films. The thickness of the thin films was also measured in order to prove the correlation between the thickness to the optical and electrical properties of the annealed thin films. Fig. 6.7 shows the 3-D AFM images of TPD:PBD:Alq_3 blend thin film with different annealing times. The surface of the thin films observed is smooth for the as-cast and tends to be rougher with the increase in the annealing time. Small grain starts to form on the 10 minutes annealed thin film and the grain size becomes larger for the 20 minutes annealed film. With measuring height of 300 nm, valleys like shape were obviously observed. The low height measurement means that the distance between the cantilevers with the surface of the thin film is very close together. Force of the cantilevers that acting on the thin film surface becomes more sensitive which gives a clearer image of surface morphology of the thin film. The valley shape turns to rock-mountain shape when the annealing time is increased to 30 minutes. These indicate that the formation of the oxide peaks increases which is caused by the attachment of oxygen molecules from air to the film during the annealing process. Similar evident was obtained from the microscopic image as shown in Fig. 6.8. There is a report which relates the formation of spots on surface of an organic thin film to crystallization process [*Park, et al., 2010*]. However, the previous XRD result shows no sign of crystallization occurring in the thin film. The small spot formation may assigned to the degradation effect which is caused by oxidation process [*Burrows et al., 1994*] as the annealing process was performed to the thin films. The small spot (in the box) starts to form after 20 minutes of annealing time. The density of the spot is observed to increase when the annealing time is increased which is due to longer time of expose to the ambient air.

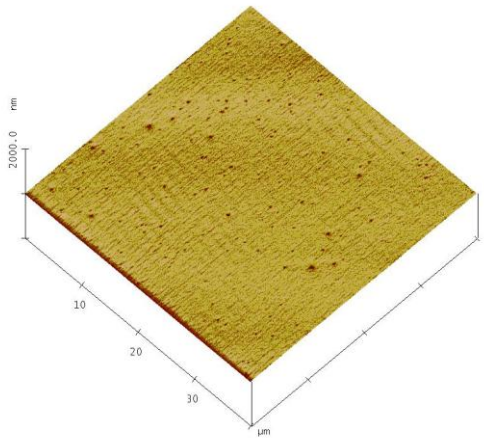

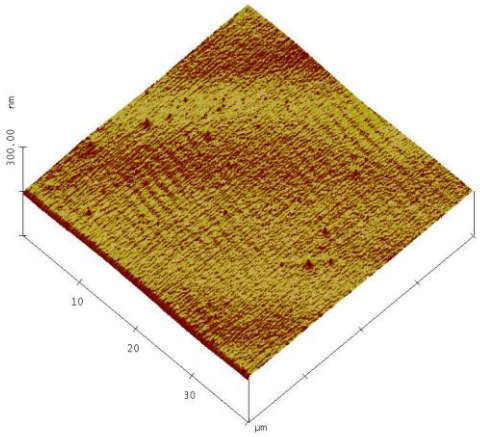

As-cast

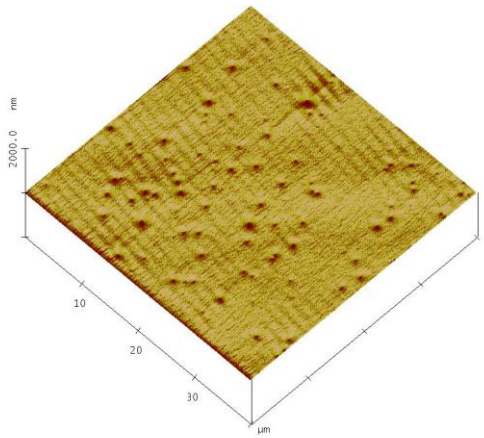

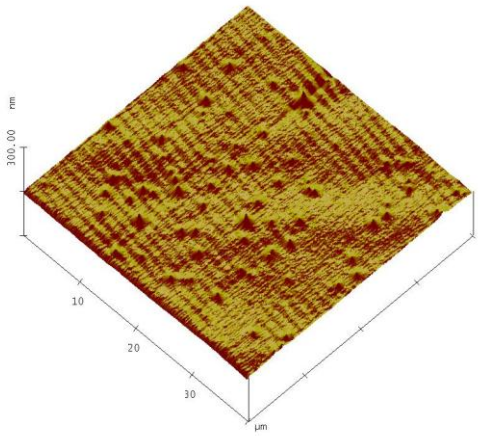

10 minutes

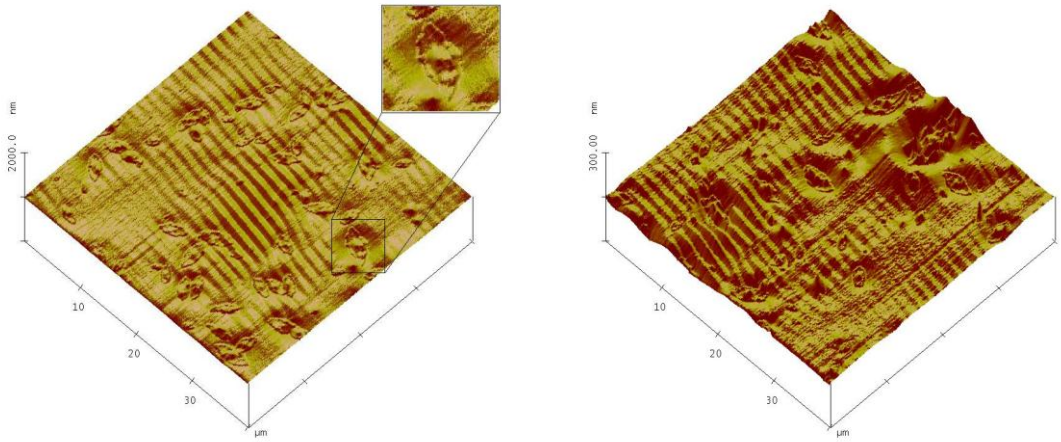

20 minutes

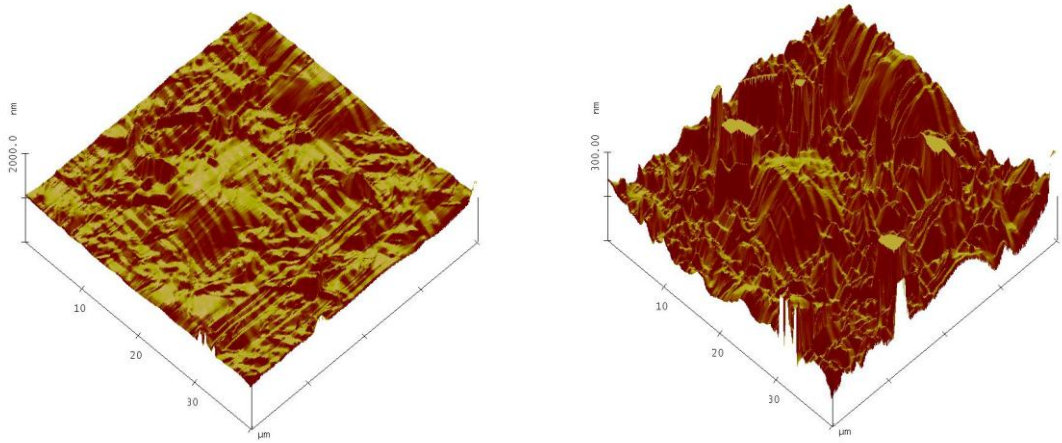

30 minutes

Figure 6.7: AFM images of blend thin film with different annealing time measured at 2000 nm (left) and 300 nm (right) heights.

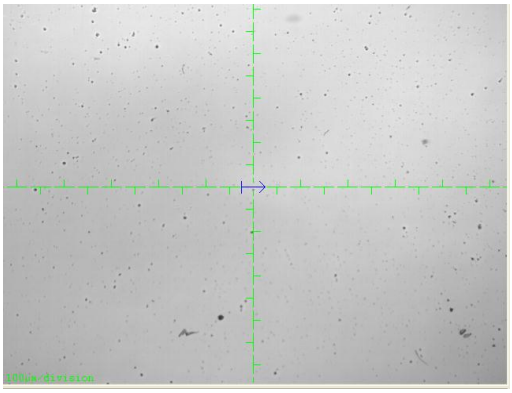

as-cast

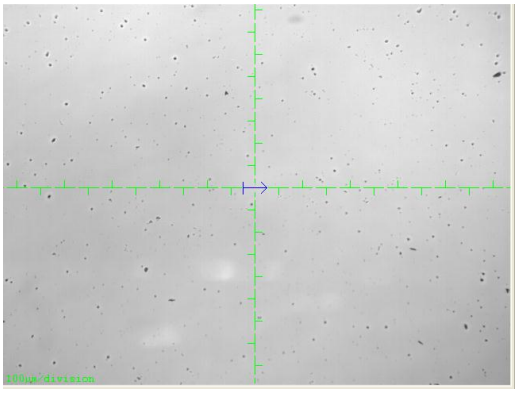

10 minutes

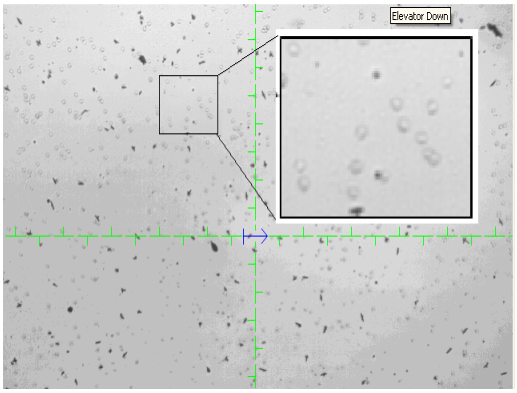

20 minutes

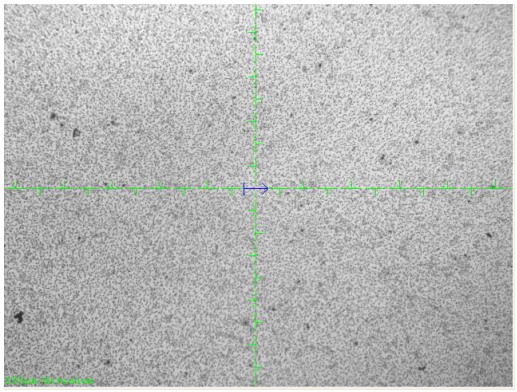

30 minutes

Figure 6.8: Microscopic image of as-cast and annealed device at different annealing time

The thickness of the thin films measured decreased as the annealing time is increased as similarly reported in [*Lee et al., 2010*]. This result supports the optical analysis in the previous section (section 6.4). As heat energies are applied, the molecules in the organic thin film reorganize themselves to become a more compact structure. As a result, the thickness of the thin film reduces gradually. The reorganization of the molecules may depend on the annealing temperature and time [*Caria et al., 2006*]. In this work, the annealing process was performed at a fixed temperature of 100^{o}C in an ambient air which has caused the blend thin film to be

exposed to oxygen and encouraged oxidation process to occur which will influence the surface roughness of the film. Thus, the annealing time is a critical parameter that can be used to control the degradation process in an open air annealing process. Fig. 6.9 shows the relationship between the roughness and the thickness of the blend thin film with different annealing time. Reduction in thickness as annealing time increases due to compactness of the structure but the increase in roughness is due to the oxidation process increases as the annealing time increases.

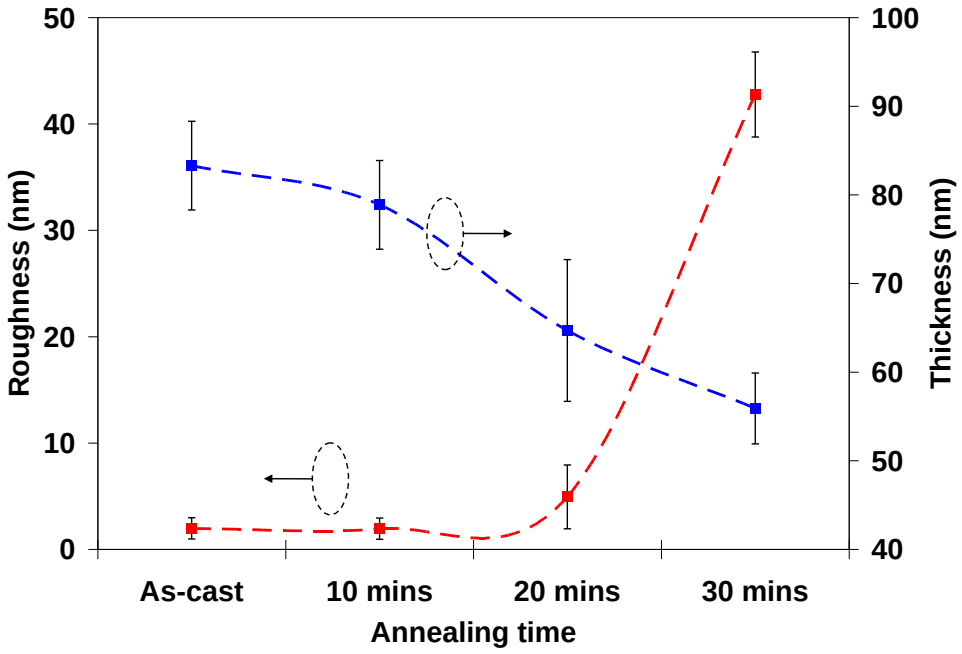

Figure 6.9: Roughness and thickness of blend thin film with different annealing time

6.6 Electroluminescence Study

After performing the annealing process, the device performance of TPD:PBD:Alq_3 based single layer OLED has been characterized. Fig. 6.10 shows the *J-V* characteristics of the devices annealed at different annealing times. The unique *J-V* characteristic of the as-cast blend OLED observed to be shifted towards higher driven voltage. Current density of the devices increases with the increase in annealing time in the voltage region from 6 to 9V. The breakdown voltage of the devices increase to a higher voltage for the device annealed at 10 and 20 minutes and then decreases to a

lower voltage for the 30 minutes annealed device. This indicates that the Joule heating rapidly occurs for the device annealed at 30 minutes due to the degradation process which has been confirmed by the previous AFM results.

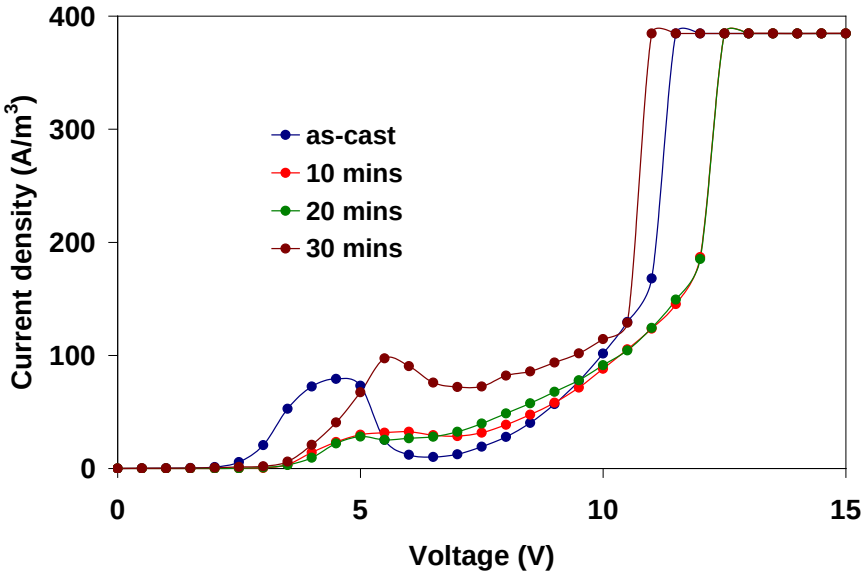

Figure 6.10: *J-V* characteristic of the blend thin films annealed at different annealing times

In order to study the injection properties of the OLED devices, Fowler-Nordheim (F-N) tunneling injection theory has been applied. As briefly discussed in Chapter 2, F-N theory depends on the effective barrier height between HOMO or LUMO level to anode and cathode work function, respectively. By plotting $\ln(J/F^2)$ versus 1/F, the properties of a barrier height can be determined. Fig. 6.11 (a) shows the F-N plot of the blend thin films with different annealing time. One can see that at low electric field, the *K* value increases for the device annealed at longer annealing time and consequently, the barrier height Φ also increases [*Parker, 1994*]. This result is supported by the previous AFM results. The interfacial oxide layer that the formed on the organic surface during the annealing process has caused a poor charge injection from the aluminum metal to the organic layer. More formation of the oxidation layer at

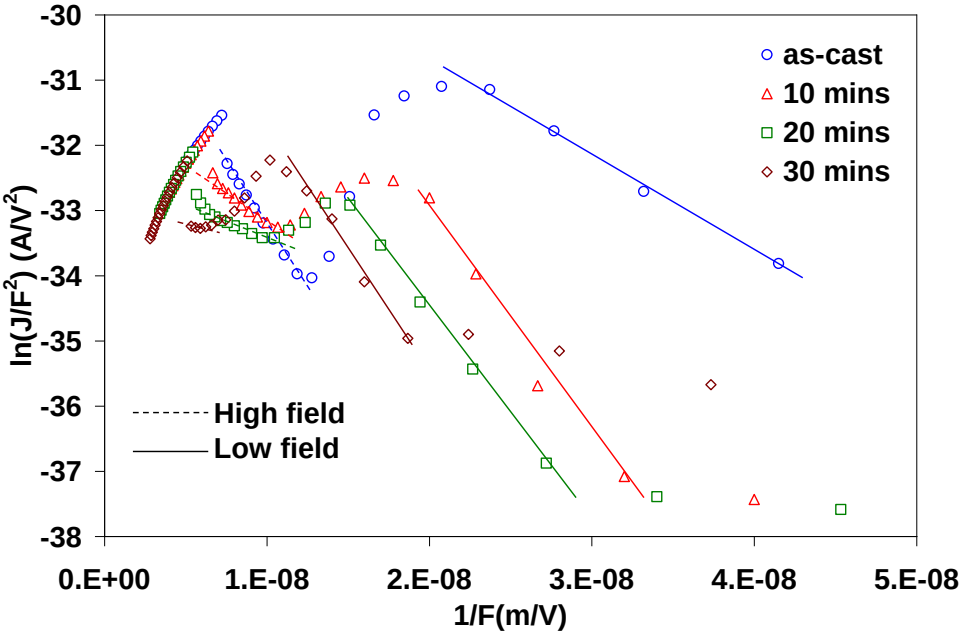

(a)

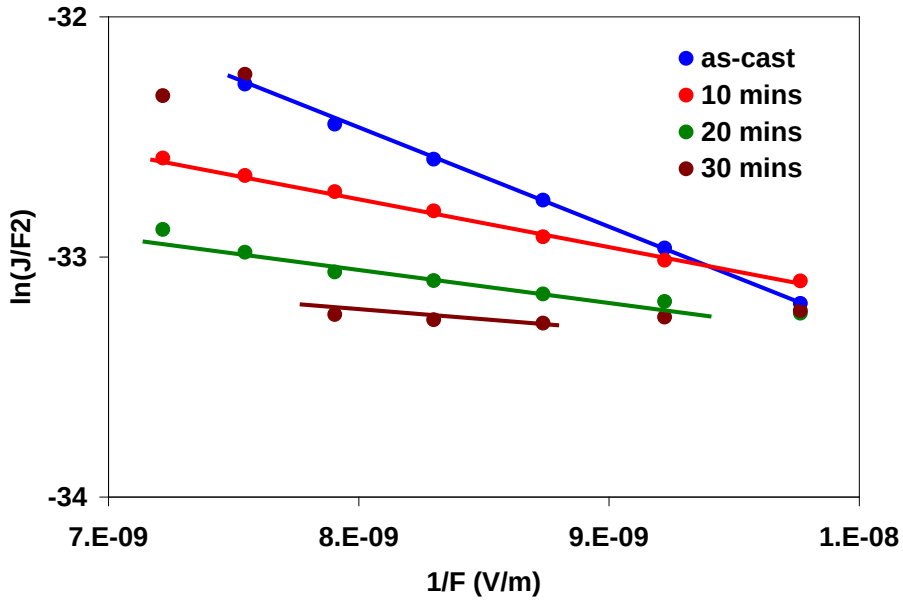

(b)

Figure 6.11: (a) F-N plot of blend thin film with different annealing time. (b) F-N plot at high voltage range

longer annealing time has caused deterioration in the injection mechanism. However, vice versa characteristic is observed at a much higher electric field as shown in Fig. 6.11 (b). The barrier height is reduced in the device that was annealed at longer annealing time. This is probably due to the lower thickness of the organic blend where the effects of oxidation layer can be neglected.

Log J-Log V graph has been plotted to further analyze the electrical properties of the annealed blends OLED. Fig. 6.12 shows *Log J-Log V* plot of the single layer OLED annealed at various annealing times. In low voltage region (Ohmic), the value of *m* observed is increased from 1.6 for the as-cast thin film to 2.5 for the 10 minutes annealed OLED. This indicates that the carriers are transported efficiently in the organic layer at Ohmic region for the 10 minutes annealed OLED due to the compact molecular structure after the annealing process. The value of *m* slowly decreases for the thin film annealed at higher annealing time with the *m* value of 1.8 and 1.3 for the 20 and 30 minutes annealing time, respectively. The decrease in the *m* values for the sample annealed at higher annealing time may be caused by the degradation process that has been proven by the previous AFM results.

A similar phenomenon was observed at SCLC region. For the as-cast OLED, the value of m ≈ 6.8, and then it increases to a maximum value of 11.1 for the OLED annealed for 10 minutes. The value of *m* decreases to 8.7 and 7.6 for the 20 and 30 minutes annealed OLED, respectively. At this stage, the carriers are highly transported due to higher voltage supplied.

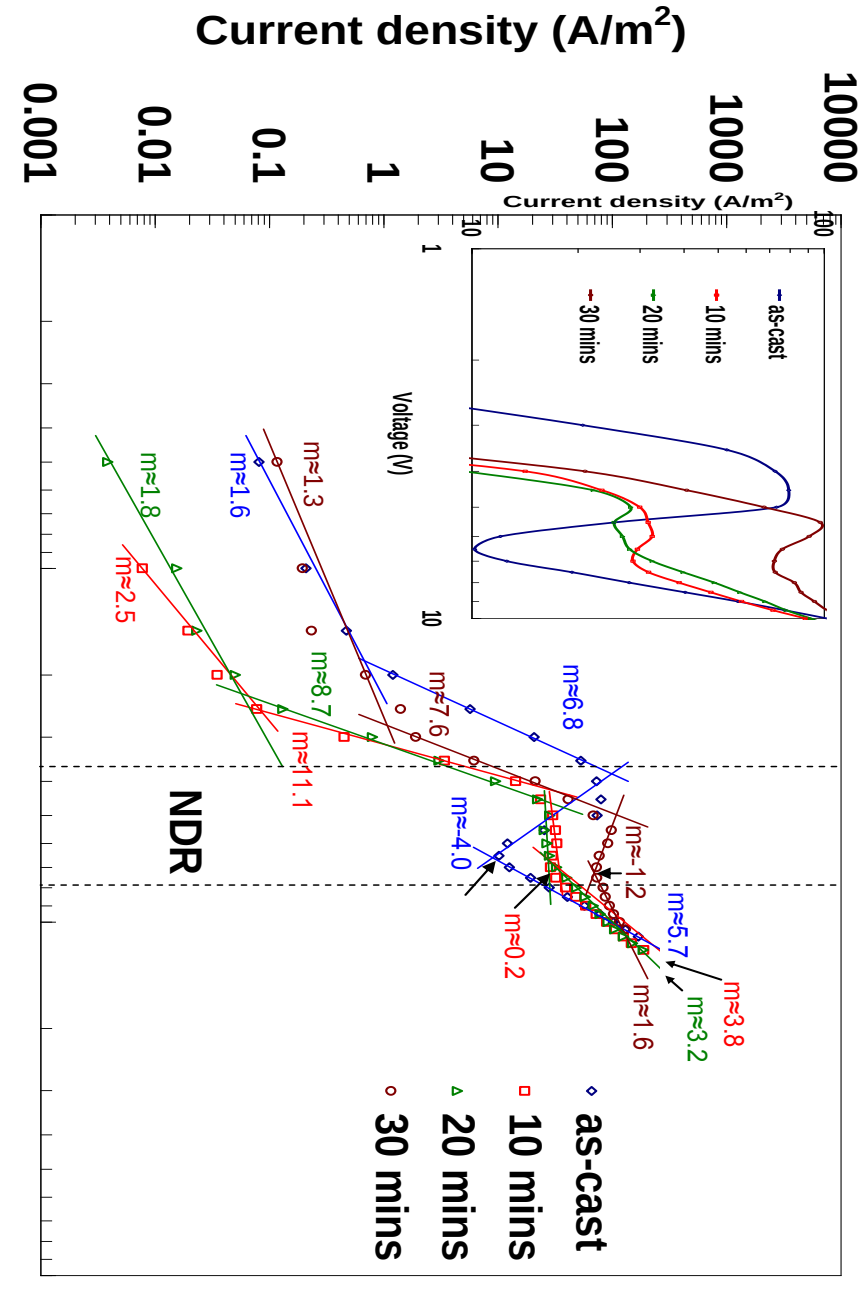

Figure 6.12: Log J-Log V plot of single layer OLED annealed with various annealing time. The insert is the clear feature of NDR.

As the voltage supplied is increased, carriers are accumulated in the organic layer to form space charges and light are emitted due to radiative recombination process. The current density observed drops which gives negative value of *m* in NDR region for the as cast OLED. This phenomenon has been discussed at length in the previous chapter and it is due to phonon scattering induces by guest hopping side (GSH). However for the 10 minutes annealed OLED, the *m* value obtained is a positive value of 0.2. This indicates that the phonon scattering effect does not occur and carriers are freely transported to the respective electrode. This may due to the improvement in the molecular structure of the thin film during the annealing process where the rearrangement of molecules has reduced the GHS formation in the blend thin film. However, at higher annealing time, the *m* value is -1.2. It is postulated that GSH is reformed at a higher annealing time. Thus the transported carriers are trapped in the generated GHS and recombined to release phonon energy. The phonons scatter the carriers, thus causing a slight reduction in the current density. At a higher voltage (higher than 9 V), the transportation mechanisms of the OLED device can be described as TCLC. There is a significant change in the TCLC region where the value of *m* observed is decreased with the increase in the annealing time. For the as-cast OLED, the value of m≈5.7 and it drops to 3.8, 3.2 and 1.6 for the 10, 20 and 30 minutes annealed OLED. This indicates that the traps in the organic blend film have been reduced with the annealing process [*Foreman et al., 2010*] which results in the compact structure and low in thickness.

Luminance data was obtained simultaneously with the electrical data under the forward bias voltage. Fig. 6.13 shows the *L-V* characteristic of the blend OLED annealed at different annealing times. The turn on voltage of the device observed increases for the annealed OLED device. This may occur due to poor injection

properties of the metal-organic interface of the aluminum and the blend thin film. Annealing under an ambient air could expose the organic layer to the oxidation process which has been proven by the AFM images. The surface become rougher due to oxidative degradation process of the organic thin films annealed with longer annealing time. Poor quality of the surface morphology of the thin film may also reduce the injection efficiency between the aluminum electrode and the organic layer after the aluminum electrode was deposited on top of it. There is a significant increase in the luminance for the 10 and 20 minutes annealed OLED after 11V which indicates that recombination that occurs in TCLC region are greater then that in SCLC region for the particular devices. The maximum luminance of the annealed OLED devices obtained to be higher for 10 minutes annealing time with luminance of 680±17 cd/m^2. It is almost two times higher than the as-cast OLED with luminance of 347±10 cd/m^2. However, further increase in the annealing time has caused the luminance to be reduced due to degradation of the device.

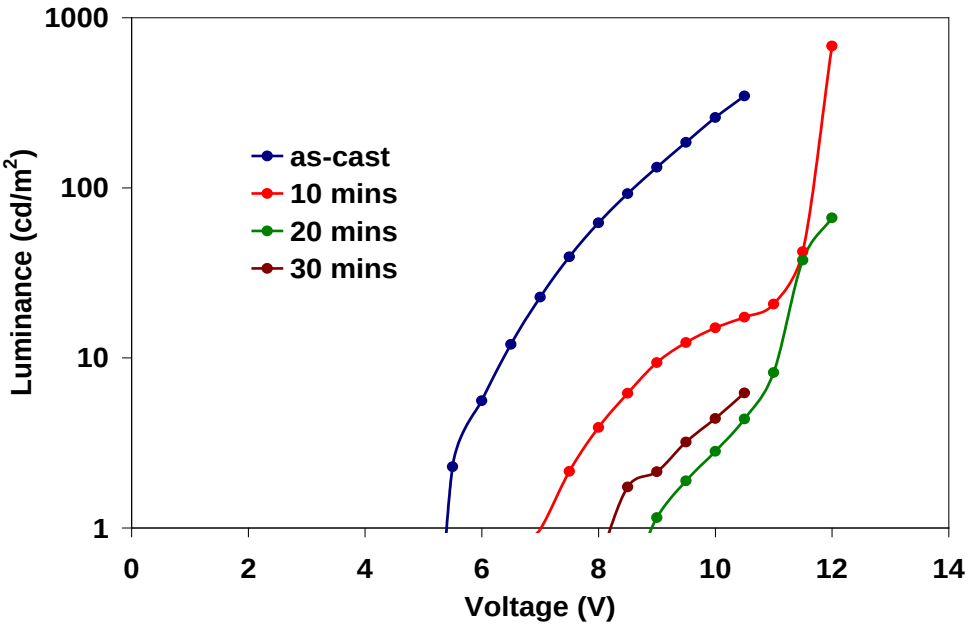

Figure 6.13: *L-V* characteristic of blend OLED with different annealing time

Current efficiency, η, observed is higher for the 10 minutes annealed OLED with η = 3.7±0.7 which is 0.33% higher than that of the as-cast OLED. However, the current efficiency of the devices reduces gradually for higher annealing time. Relationship between maximum luminance and current efficiency with annealing time is shown in Fig. 6.14. It is noted that the current efficiency is strongly dependence on luminance of the devices as the current density shows almost similar results for all the annealed OLED. The performance of the annealed OLED devices is tabulated in Table 6.2.

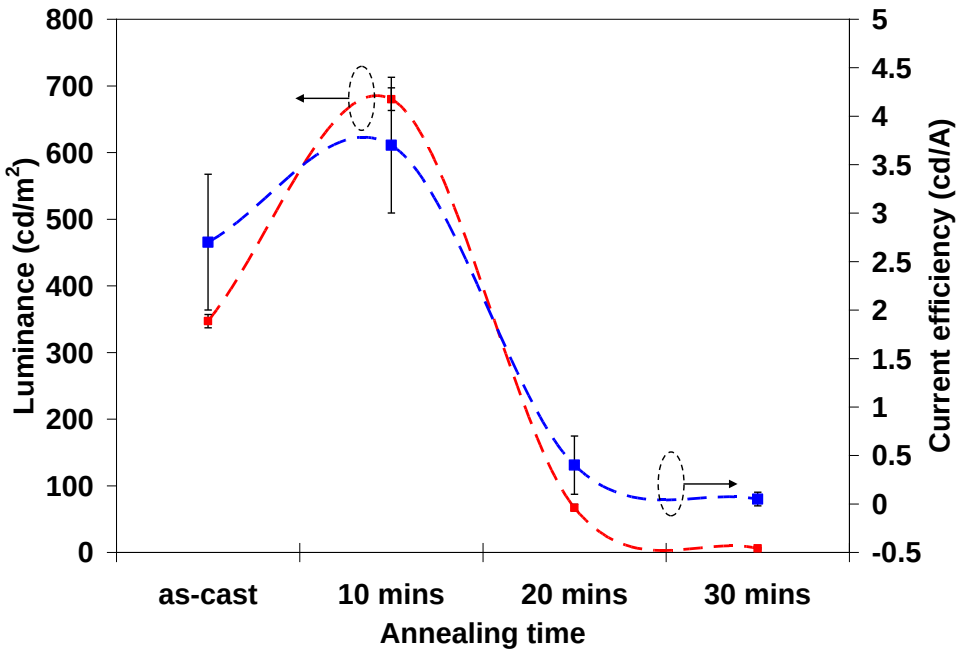

Figure 6.14: Maximum luminance and current efficiency of single layer OLED with respect to annealing time

Table 6.2: Performance of annealed blend OLED

	Annealing time, *t* (min)					
	as-cast	3	5	10	20	30
V_{on} (±0.5 V)	5.0	5.0	7.0	7.0	9.0	8.0
V_{off} (±0.5 V)	11.5	10.5	12.0	12.5	12.5	11.0
J_{max} (±0.2 A/m^2)	384.6	384.6	384.6	384.6	384.6	384.6
L_{max} (cd/m^2)	347±10	552±11	378±12	680±17	67±5	6±1
η_{max} (cd/A)	2.7±0.7	2.7±0.4	2.0±0.6	3.7±0.7	0.4±0.3	0.05±0.04

Fig. 6.15 shows CIE plot of the blend device with different annealing time. It is importance to see that all devices exhibit an emission of green color which is similar to the PL result. The CIE coordinates was shifted from (0.29,0.52) for the as-cast OLED to (0.30,0.52) for the OLED annealed for 10 minutes. The coordinates was than returned to the as-cast position for the 20 minutes annealing before shifted upward to the position of (0.29,0.56) for the 30 minutes annealing time. These translations occurred around the green color region, which indicates that the Alq_3 remained as the center of luminescence for the blend OLEDs.

The luminance-current density (*L-J*) characteristic has been plotted to study the turn on current on the annealed devices. Fig. 6.16 shows the *L-J* plot of the annealed OLEDs. The 10 minutes annealed device shows a slight reduction in the turn on current with a value of 28.5±0.2 A/m^2. This is believed related to the reduction in the GHS generation due to the annealing process. Above this optimum annealing time, the OLED exhibits high turn on current which indicates the poor injection mechanism due to the degradation of the device.

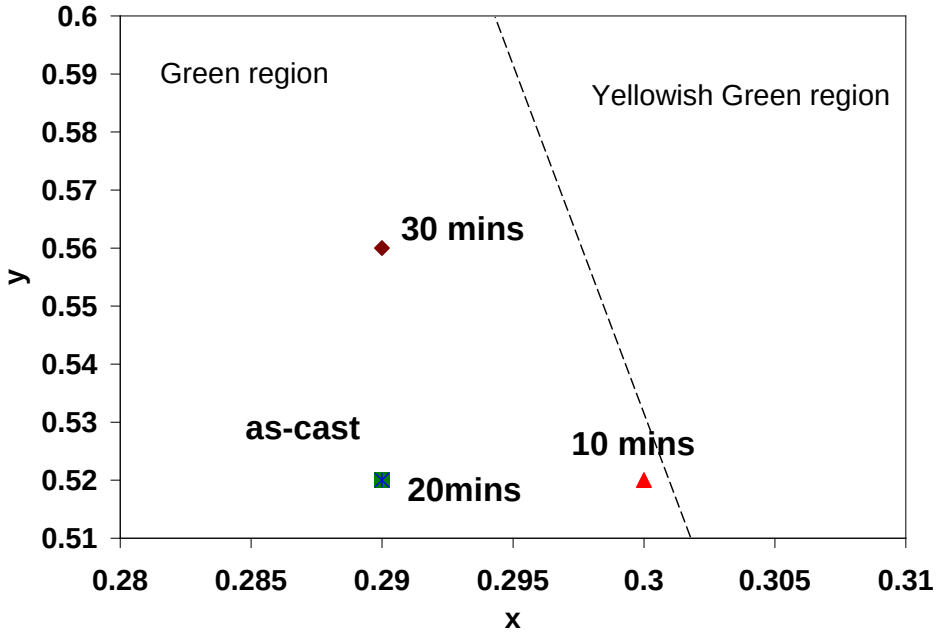

Figure 6.15: CIE plot of the blend OLED with different annealing time.

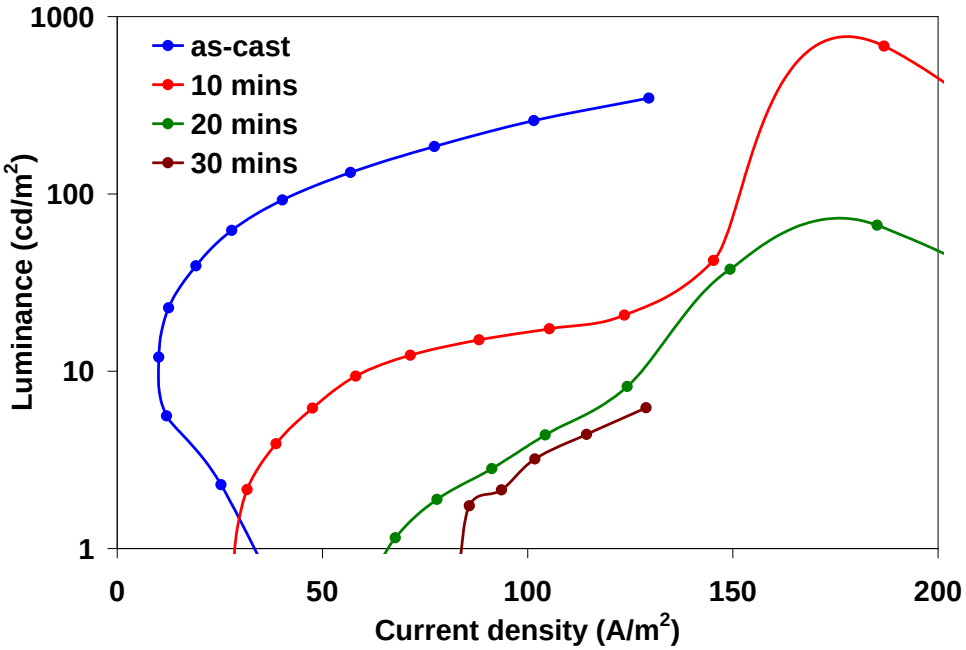

Figure 6.16: *L-J* characteristic of blend OLED with different annealing time

6.7 Summary

Effects of annealing on the novel blends OLED has been investigated. FTIR results show that the blend thin film started to degrade after 20 minutes of annealing time. The thin film shows an amorphous structure at all annealing time. The optical study indicates that the absorption of the thin film is reduced and the PL intensity is increased due to the reduction in the thickness of the thin films as the annealing time is increased. Investigation of the surface morphology of the thin film by AFM confirms the degradation of the thin film is formed after 20 minutes of annealing time as can be seen from the increase in the surface roughness of the blend film. Electrical and luminescence study of the annealed devices show that the turn on voltage of the devices is increased with the increase in the annealing time. In contrast, the effect of the negative differential resistance (NDR) is reduced with the annealing time. The highest maximum luminance and current density is obtained for the blend OLED which has been annealed for 10 minutes. The device shows degradation at a longer annealing time.

References

Adachi, C., Nagai, K., & Tamoto, N. (1995). Molecular Design of Hole Transport Materials for Obtaining High Durability in Organic Electroluminescent Diodes. Applied Physics Letters, 66, 2679-2681.

Burrows, P. E., Bulovic, V., Forrest, S. R., Sapochak, L. S., McCarty, D. M., & Thompson, M. E. (1994). Reliability and Degradation of Organic Light Emitting Devices. Applied Physics Letters, 65, 2922-2924.

Caria, S., Da Como, E., Murgia, M., Zamboni, R., Melpignano, P., & Biondo, V. (2006). Enhanced Light Emission Efficiency and Current Stability by Morphology Control and Thermal Annealing of Organic Light Emitting Diode Devices. Journal of Physics Condensed Matter, 18, S2139-S2147.

Choudhury, K. R., Lee, J., Chopra, N., Gupta, A., Jiang, X., Amy, F., et al. (2009). Highly Efficient Hole Injection Using Polymeric Anode Materials for Small-Molecule Organic Light-Emitting Diodes. Advanced Functional Materials, 19, 491-496.

Foreman, J. V., Everitt, H. O., Yang, J., McNicholas, T., & Liu, J. (2010). Effects of Reabsorption and Spatial Trap Distributions on the Radiative Quantum Efficiencies of ZnO. Physical Review B, 81, 115318.

Jeong, W. I., Kim, S. Y., Kim, J. J., & Kang, J. W. (2009). Thickness Dependence of PL Efficiency of Organic Thin Films. Chemical Physics, 355, 25-30.

Kim, W. H., Kushto, G. P., Kim, H., & Kafafi, Z. H. (2003). Effect of Annealing on the Electrical Properties and Morphology of a Conducting Polymer Used as an anode in Organic Light-Emitting Devices. Journal of Polymer Science Part B: Polymer Physics, 41, 2522-2528.

Krieg, T., Petr, A., Barkleit, G., & Dunsch, L. (1999). Improved Thermal Stability of Nonpolymeric Organic Glasses by Doping with Fullerene C60. Applied Physics Letters, 74, 3639-3641.

Kulkarni, A. P., Tonzola, C. J., Babel, A., & Jenekhe, S. A. (2004). Electron Transport Materials for Organic Light-Emitting Diodes. Chemistry of Materials, 16, 4556-4573.

Lee, H., Kim, A., Cho, S. M., & Chae, H. (2010). Characterization of Thermal Annealing of Gravure Printed PVK/Ir(Ppy)3 Organic Light Emitting Layers. Current Applied Physics, 10, e143-e146.

Li, J.-H., Huang, J., & Yang, Y. (2007). Improved Hole-Injection Contact for Top-Emitting Polymeric Diodes. Applied Physics Letters, 90, 173505-173503.

Muhammad, F. F., & Sulaiman, K. Effects of Thermal Annealing on the Optical, Spectroscopic, and Structural Properties of Tris (8-Hydroxyquinolinate) Gallium Films Grown on Quartz Substrates. Materials Chemistry and Physics, In Press, Corrected Proof.

Osipov, K. A., Pavlovskii, V. N., Lutsenko, E. V., Gurskii, A. L., Yablonskii, G. P., Hartmann, S., et al. (2007). Influence of Thermal Annealing on Photoluminescence and Structural Properties of N,N'-diphenyl-N,N'-bis(1-naphthylphenyl)-1,1'-biphenyl-4,4'-diamine ([alpha]-NPD) organic thin films. Thin Solid Films, 515, 4834-4837.

Park, S.-W., Choi, J.-M., Lee, K. H., Yeom, H. W., Im, S., & Lee, Y. K. (2010). Amorphous-to-Crystalline Phase Transformation of Thin Film Rubrene. The Journal of Physical Chemistry B, 114, 5661-5665.

Parker, I. D. (1994). Carrier Tunneling and Device Characteristics in Polymer Light Emitting Diodes. Journal of Applied Physics, 75, 1656-1666.

Ribierre, J. C., Yates, C. J., Ruseckas, A., Staton, S. V., Burn, P. L., & Samuel, I. D. W. (2010). Effects of Solution Processing and Thermal Annealing on The Phosphorescence of Iridium(III) Complex-Cored Dendrimer Films. Organic Electronics, 11, 62-66.

Sepeai, S., Salleh, M. M., Yahaya, M., & Umar, A. A. (2009). Improvement of White Organic Light Emitting Diode Performances by an Annealing Process. Thin Solid Films, 517, 4679-4683.

Singh, R., Kumar, J., Singh, R. K., Kaur, A., Sood, K. N., & Rastogi, R. C. (2005). Effect of Thermal Annealing on Surface Morphology and Physical Properties of Poly(3-Octylthiophene) Films. Polymer, 46, 9126-9132.

Song, M., Park, J., Yoon, M., Yoon, H., Kim, A., Jin, S.-H., et al. (2010). Synthesis and Characterization of Poly(Carbazolyl-2,7-Vinylene) Derivatives for Organic Light-Emitting Diode Applications. Macromolecular Research, 18, 1088-1095.

Sun, M.-C., Jou, J.-H., Weng, W.-K., & Huang, Y.-S. (2005). Enhancing the Performance of Organic Light-Emitting Devices by Selective Thermal Treatment. Thin Solid Films, 491, 260-263.

Tokito, S., Tanaka, H., Noda, K., Okada, A., & Taga, Y. (1997). Temperature Dependences of Electroluminescent Characteristics in the Devices Fabricated with Novel Triphenylamine Derivatives. Electron Devices, IEEE Transactions on, 44, 1239-1244.